Cellular cholesterol regulates monocyte deformation

Amit K. Saha[a], Shatha F. Dallo[a], Ariana L. Detmar[a], Pawel Osmulski[b], Maria Gaczynska[b], Tim Hui-Ming Huang[b], Anand K. Ramasubramanian[c*]

[a]Department of Biomedical Engineering, The University of Texas at San Antonio, San Antonio, Texas, United States of America

[b]Department of Molecular Medicine, The University of Texas Health Science Center at San Antonio, San Antonio, Texas, United States of America

[c]Department of Biomedical, Chemical and Materials Engineering, San José State University, San José, California, United States of America

[*]Correspondence to: Department of Biomedical, Chemical and Materials Engineering, San José State University, CA 95192-0082, USA. Tel.: +1 (408) 924-3922.

anand.ramasubramanian@sjsu.edu

Abstract

The role of cholesterol content on monocyte biomechanics remains understudied despite the well-established link between cholesterol and monocytes/macrophages in atherosclerosis, and the effect on other cell types. In this work, we have investigated the effect of cholesterol on monocyte deformability and the underlying molecular mechanisms. We altered the baseline cholesterol in human monocytic cell line THP-1, and investigated the changes in monocyte deformability using a custom microfluidic platform and atomic force microscopy. We observed that the cholesterol depletion lowered deformability while enrichment increased deformability compared to untreated cells. As a consequence of altered

deformability, cholesterol depleted cells spread more on collagen-coated surfaces with elongated morphology, whereas cholesterol enriched cells had a more rounded morphology. We observed that the decreased deformability in cholesterol depleted cells, despite an increase in the fluidity of the membrane, is due to an increase in phosphorylation of Protein Kinase C (PKC), which translates to a higher degree of actin polymerization. Together, our results highlight the importance of biophysical regulation of monocyte response to cholesterol levels.

Keywords

Microfluidics; Cytoskeleton; Cell deformability; Spreading; Membrane fluidity; Cell stiffness

Introduction

Cholesterol plays an important role in maintaining the integrity and functionality of plasma membrane and also the cytoskeleton (Roduit et al., 2008). As a result, cholesterol has been shown to modulate cell stiffness (H. Oh, Mohler, Tian, Baumgart, & Diamond, 2009), as well as affect various cellular processes such as protein sorting (Lundbaek, Andersen, Werge, & Nielsen, 2003), cell signaling (Foster et al., 2013; Pande, 2000; Shima, Nada, & Okada, 2003b), spreading and chemotaxis in various cell types including fibroblasts, endothelial and epithelial cells. Although the importance of cholesterol in atherosclerosis is well established, the effect of cholesterol on monocyte biomechanical response has not been studied. In this work, we tested the hypothesis that cellular cholesterol content modulates the biomechanical properties of human monocytes. To this end, we estimated the mechanical properties of naïve, cholesterol depleted and cholesterol enriched THP-1 cells. We observed that the depleted cells had lower deformability, and enhanced ability to spread and move in response to chemotaxis. Cholesterol enrichment had antithetical effects.

Materials and Methods

Cell Culture and cholesterol treatment

Human monocyte cell line, THP-1 (ATCC) was cultured in RPMI 1640 (ATCC) supplemented with 10% FBS and .05 mM mercaptoethanol (Sigma-Aldrich), at 37°C and 5% CO_2. The cells were passaged into fresh media when the cells reached a density of 10^6/ml. The cell viability was measured by trypan blue exclusion assay using the Countess automated cell counter (Life Technologies).

Cholesterol depletion was performed using Methyl-β-cyclodextrin (MβCD; Sigma-Aldrich) and enrichment using MβCD-cholesterol complex starting with stock solutions at 200 mM and 25 mM, respectively. Cells were washed once with RPMI and centrifuged at 130xG for 7 minutes at room temperature (RT), and resuspended at a concentration of $1x10^6$/ml in RPMI. Desired concentration of either MβCD or MβCD-cholesterol solution was mixed with the cell suspension, and incubated for 30 mins. at 37° C and 5% CO_2. After 30 minutes, cell viability was measured using the trypan blue exclusion assay. The cell suspension was centrifuged at 130xG for 7 minutes at RT, and then resuspended at a concentration of $1x10^6$/ml in RPMI. This was repeated thrice, and cell viability was measured again. The cell suspension was centrifuged one more time. The supernatant was discarded and the cells were resuspended in suitable media and concentration as required by a particular assay. Before utilizing the cells for any assay, the cell viability was assessed one more time.

Cholesterol content measurement

Cholesterol content in the cells was measured using Amplex Red Cholesterol Assay Kit (Life Technologies), as per the manufacturer's protocol. Approximately $0.75x10^5$ cells were used per well of a 96 well plate (Corning Inc.). The fluorescence intensity was measured at 540 nm(excitation)/600 nm(emission) using a Synergy2 plate reader (Biotek). For assessment of the total cellular content, the cells were lysed using sonication. The cells were centrifuged at 130G for 7 min, resuspended in PBS at 10^6/ml and vortexed for 60 s. After repeating this process thrice, the cells in PBS were sonicated for 90 s (Branson SLPe digital sonifier), centrifuged, resuspended in PBS, and vortexed for 45 s. This process was

repeated three times, and the cell lysate was tested for cholesterol content. For the plasma membrane cholesterol estimation, they were left intact. The cholesterol contents were determined from a standard curve using 1-20 μg/ml cholesterol standards (the cholesterol standard provided in the kit was used as reference to obtain the standard curves) and for each well plate, individual standard curves were obtained.

High throughput microfluidic device for assessing cellular deformability

A high throughput microfluidic device was fabricated for investigating single cell deformability. The design for the microfluidics platform was made using mechanical computer aided design software SolidWorks (Dassault Systèmes SolidWorks Corporation). Chrome-on-glass photo-mask was obtained from an industrial firm (Photo Sciences Inc.) based on the design. The designed pattern was transferred to silicon wafers using standard photolithographic techniques. The negative photoresist used was SU-8 2000 (MicroChem). The test channels in the device had a cross-section area of 5μmx5μm. The silicon mold was used to make polymeric micro-channels using Polydimethysiloxane (PDMS; Dow Corning). The PDMS blocks with the embedded micro-channels were attached to clean glass slides (Fisher Scientific) using oxygen plasma treatment (Harrick Plasma). Silicon connector kits (Cole-Parmer) were used so as to get better adhesion with PDMS. The channels were passivated by perfusing 5% HSA and washed with PBS.

A custom nitrogen based delivery system was used to deliver the cell suspensions at a concentration of 0.75×10^6/ml. High speed videos were taken at 20X and 40X magnifications (Leica Microsystems) using a high speed sCMOS camera (PCO-Tech) and subsequent image processing using ImagePRO (Media Cybernetics Inc.) was done. For each experiment, at least three microfluidic devices were used per condition, and at least 400-500 cells were tested per device. Cholesterol depleted cells and untreated control were used to obtain information on the role of cholesterol content on the overall cellular deformability.

Immunoblotting using anti-phosphorylation (PY 20) antibodies

Western analysis was performed using an antibody for activated (phosphorylated) PKC to determine if cholesterol treatment activates this signaling pathway. Treated and untreated THP1 cells were washed and centrifuged at 150xg for 7 minutes. Then, $2x10^6$ cells were treated with MCP-1 for 2.5 minutes. Cells were washed and collected by centrifugation at 150xg for 7 minutes. Supernatant was removed and cells were resuspended in 100 µL RIPA buffer (25mM Tris-HCl pH 7.6, 150mM NaCl, 1% NP-40, 1% sodium deoxycholate, 0.1% SDS; Thermofisherscientific) containing protease and phosphatase inhibitor cocktail at a dilution of 1:9 (Abcam). The lysates were placed on ice for 10 min and centrifuged at 13, 000x g for 5 minutes to remove cell debris. Protein lysate samples (40 µL) were boiled in loading buffer (0.1 M Tris, pH 6.8, 4% (v/v) SDS, 20% (v/v) glycerol, 0.2% (w/v) bromophenol blue, 10 mM DTT) for 5 min, and samples were electrophoresed using 8% (w/v) SDS polyacrylamide reducing gels in Laemmli buffer (0.0255 M Tris, 0.25 M glycine, 0.1% (w/v) SDS, pH 8.3). The proteins were transferred onto PVDF membranes (BIO RAD) in Tris-Glycine SDS buffer (25 mM Tris, 40mM Glycine, 3.75ml of 10% SDS, 20% (v/v) methanol). The membrane was blocked with 5% (w/v) BSA in TBS-Tween 20 (0.05 M Tris, 0.25 M NaCl, pH 7.4, 0.05% (v/v) Tween-20) for 1 h at room temperature to prevent non-specific binding. Western immunoblotting for signaling molecules was performed using primary anti-human antibodies (Santa Cruz Biotechnology, Inc.) mouse anti-p -Tyr (PY 20) at a dilution of 200ug/ml. Mouse anti-actin (Invitrogen) was used to demonstrate even protein loading. The PVDF membranes were incubated overnight with primary antibody at 4 ºC, (diluted in 5% (w/v) BSA (Sigma) in TBS-Tween 20). Membranes were washed 3x with TBS-Tween 20, then incubated for an hour at 1:5000 with goat anti-mouse (Pierce) horseradish peroxidase-conjugated IgG as the secondary antibody. After further washing in TBS-Tween 20 for 5 x 10 min, blots were developed using enhanced chemiluminescence (Pierce ECL western blotting substrate; Thermo Scientific) and then exposed to X-OMAT AR film (Kodak). Bands were quantitated by densitometry using a scanner and ImageJ software (NIH).

Cell morphology during chemotaxis

Monocyte chemotaxis was performed using 5µm transwell inserts (Corning) in 24 well plates. 600 µL of complete media with or without chemoattractant was put in each well. 30 ng/ml of MCP-1 (R&D) was used as chemoattractant. After 3 hours, cells passing through the transwell membrane were stained for visualization using confocal microscopy (Carl Zeiss AG). The cells attached to the membrane were fixed with a 2% Formaldehyde solution in PBS at 4°C overnight. After completion of the fixation stage, the membranes were washed with 1x Permwash (BD) prepared in PBS. The membranes were then carefully cut from the membrane using a curved surgical scalpel (Ted Pella Inc.). 0.1% Triton X (Sigma) was added for 3 minutes to permeabilize the cells (500µL per well). 0.5% BSA in 1X Permwash was added to block non-specific binding (500µL per well) for 15 minutes. Fluorescently tagged phalloidin (AF 488; Life Technologies) was added along with DAPI (Life Technologies) in 1:100 dilution in 1X Permwash (200µL per well). The membranes were incubated for 1 hour at room temperature accompanied by gentle rocking. The membranes were then washed thrice with 1X Permwash in PBS, followed by 1 rinse with PBS. The membranes were then mounted on standard glass slides, fluorosave was added and a cover slip was placed on top. The slides were then imaged at 100X magnification. Three membranes were imaged per condition for every experiment, and at least 20 cells were imaged per membrane.

Cell spreading

8-well chamber slides (ThermoFisher Scientific) were coated with 500 µL 10µg/cm^2 type 1 collagen per well (Corning Inc.). The collagen was resuspended in 0.02N acetic acid, with a final volume of 300 µL per well. The slides were left undisturbed at room temperature for 1 hour. This was followed by 2 washes using RPMI (ATCC). 50000 cells were seeded per well and the slides were left undisturbed at 37°C for 3 hours. 100 nM PMA were added to activate the THP-1 cells. Upon reaching the specific time point, the cells were washed once with PBS and fixed with 2% Formaldehyde, followed by processing for scanning electron microscopy. The cells were fixed with a solution of glutaraldehyde (2.5% w/v) in 0.1 M sodium cacodylate buffer at pH 7.4 for 2 h at 37°C. Following fixation, they were treated with a solution of osmium tetroxide (1% w/v) in 0.1 M sodium cacodylate buffer at pH 7.4 for 2 h at room temperature. The

samples were rinsed with water and soaked in a series of ethanol solutions (a step gradient of 30%, 50%, 70%, and 90% in water for 15 min per step), ending with 100% ethanol. After dehydration, the samples were dried overnight in a vacuum dryer and subsequently coated with a 60:40 gold-palladium alloy; approximately 10 nm thick using a Cressington Sputter coater for a duration of 30 sec. The cells were imaged using a Hitachi 1510 Scanning Electron Microscope, followed by subsequent image analysis. For each experiment, there were 3 chambers per condition, and at least 60 cells were analyzed per chamber.

Membrane Fluidity

Membrane fluidity was estimated using the fluorescent probe pyrenedecanoic acid (PDA; Markergene Technologies). For each condition, approximately 10^5 cells were centrifuged at 130xG for 7 mins, and the supernatant was discarded. The cells were resuspended in 300 µL perfusion buffer (Markergene Technologies) containing a 20 µM solution of PDA in 0.1% pluronic F127 (Markergene Technologies). The cells were incubated in dark for 20 mins. at room temperature. This was followed by washing with 500 µL perfusion buffer (Markergene Technologies) thrice and finally put in a 96 well plate (Corning), re-suspending the cells in a final volume of 200 µL.

Lastly, fluorescence intensity of PDA monomers and isomers were assessed using a Synergy2 plate reader (Biotek) at 360 nm (excitation) and 420 nm (emission for PDA monomer)/485 nm (emission for excimer).

Statistics

All the experiments were performed in triplicate, and each experiment was repeated at least thrice under independent conditions, on different days, unless otherwise mentioned. The results are represented as mean ± SEM from one representative experiment. Statistical differences were evaluated using either one-way ANOVA with Tukey's *post hoc* test or Students' t-test (GraphPad Prism), and significance was reported at α=0.05.

Results and Discussion

The majority of the cellular cholesterol resides in the plasma membrane and plays a vital role in maintaining the membrane structure and functionality [(Lundbaek et al., 2003; Shima, Nada, & Okada, 2003a)]. Apart from the plasma membrane, cholesterol has a global impact on the cell and also affects the cytoskeleton [(Kwik et al., 2003)]. Cholesterol has been shown to alter the membrane-cytoskeletal adhesion [(Sun et al., 2007)] and also modulate the biomechanical response in different cells like osteoblasts [(Xing et al., 2011)] and fibroblasts [(Kwik et al., 2003)].

At first we depleted the baseline cholesterol content in human monocytic cell line THP-1 cells using MβCD and estimated cholesterol levels using cholesterol oxidase based assay. The baseline cholesterol was measured as 3.25 μmol/10^6 THP-1 cells. 5 and 10 mM of MβCD was used for cholesterol depletion and we observed a decrease of 50% and 67% in cholesterol levels post treatment, respectively (Table 1). Following cholesterol treatment, viable cells were separated, and the final cell viability was estimated to be above 90%. Plasma membrane accounted for the majority of the cellular cholesterol content, with untreated and cholesterol depleted cells having ~87% and ~85% of the total cellular cholesterol in the plasma membrane, respectively.

Having successfully altered the baseline cholesterol levels in human monocytic cell line THP-1 cells, we then estimated the changes in plasma membrane fluidity due to cholesterol content. Upon interaction, the monomers of the fluorescent probe PDA form excimers, which have an emission spectra different from that of the monomers. The membrane fluidity is measured as the ratio between the excimers and the monomers, as PDA tends to aggregate when the fluidity is higher. We observed that cholesterol depletion in THP-1 cells resulted in 1.3-fold higher membrane fluidity as compared to the untreated cells (Fig. 1). The enhanced plasma membrane fluidity resulting from cholesterol depletion can be attributed to disruption of membrane lipid raft by MβCD [(Barman & Nayak, 2007)]. Cell signaling, phagocytosis and changes in

other membrane-dependent functions, are dependent on the membrane fluidity which is indirectly controlled by the cell health, cytoskeletal distribution and the overall fluidity of the cell (Helmreich, 2003).

Even though the majority of the cholesterol resides in the plasma membrane, its effects are not restricted to the plasma membrane alone. Cellular cholesterol has a global effect on the cell (Kwik et al., 2003). Cholesterol has been shown to significantly alter the deformability of cells such as endothelial cells (Byfield et al., 2004) and neutrophils (H. Oh et al., 2009). Significant changes in cell deformability can be observed in different diseases such as malaria (Shelby, White, Ganesan, Rathod, & Chiu, 2003), cancer (Xu et al., 2012) and atherosclerosis (Hayashi & Higaki, 2016). Assessment of cell stiffness is performed using a variety of techniques such as atomic force microscopy (AFM) (Thomas, Burnham, Camesano, & Wen, 2013), optical tweezers (Dy, Kanaya, & Sugiura, 2013) and micropipette aspiration (K. W. Oh, Lee, Ahn, & Furlani, 2012). While these techniques offer accurate insights, they are significantly low throughput. In this work, we developed a high throughput microfluidic device to investigate the mechanical properties of the cell. Microfluidic channels exhibit resistance behavior similar to electrical circuits (K. W. Oh et al., 2012), and hence the eight test channels in parallel help in decreasing the resistance to flow. Also, the 2 bypass channels (50 μm width) in parallel further decrease the resistance to flow and increased the overall throughput. The test channels in our device had a dimension of 5μmx5μm, which caused the cells to deform while passing through them (Fig. 2A, Fig. S1). "Entry time" is the time a cell takes to completely deform and enter the 5 μm test channel. "Average transit velocity" is the velocity of the cell as it passes through the test channel. "Elongation index" is the ratio between the initial cell diameter and the major axis of the cell inside the test channel. We observed that cholesterol depletion resulted in an increased entry time (10 fold), but decreased average transit velocity (~50%) and elongation index (~70%) (Fig. 2B). Collectively, this shows that cholesterol depletion results in a decrease in cellular deformability.

Multiple lines of evidence relate elevated cholesterol levels to atherosclerosis [Liu, Reilly, Casasanto, McKenzie, & Williams, 2007; Mason, Herbette, & Tulenko, 1993]. Hence, we increased cellular cholesterol by treatment with 0.5 mM MβCD-cholesterol complex, resulting in a 2.7-fold enrichment (3.42±0.08 μg/ml, n=3) of total cellular cholesterol. We investigated the effect of cholesterol on cellular biomechanics using membrane fluidity assay and AFM. We estimated that the cholesterol enrichment resulted in 1.7-fold decrease in membrane fluidity compared to untreated control (1.14±0.13, n=3). We found that cholesterol enriched cells had a 1.7–fold lower Young's modulus as compared to untreated control, whereas cholesterol depletion resulted in a 1.9–fold increase (Fig. S2). Together, our data indicates that cellular deformability is substantially increased with an increase in cholesterol content.

To obtain a molecular understanding of the changes in cellular deformability, we assessed the differences in cytoskeletal rearrangement via estimation of Protein Kinase C (PKC) levels. PKC is a family of kinases located in the cytoplasm of the cell, which when activated, modifies various cellular functions through phosphorylation of target substrates [Mellado et al., 1998], and has also been shown to promote pro-atherogenic phenotypes[Rask-Madsen & King, 2005]. Cholesterol depletion has been shown to activate PKC via disruption of lipid rafts [Cabrera-Poch, Sanchez-Ruiloba, Rodriguez-Martinez, & Iglesias, 2004; Kabouridis, Janzen, Magee, & Ley, 2000], which in turn activates the cytoskeletal protein actin causing it to polymerize. Changes in actin polymerization eventually translate to changes in cell spreading [Bunnell, Kapoor, Trible, Zhang, & Samelson, 2001; Etienne & Duperray, 2011] and cell stiffness [Salker et al., 2016]. We observed that cholesterol depleted cells exhibited 25-fold higher expression of phosphorylated PKC as compared to untreated THP-1 cells (Fig. 3). The enhanced actin polymerization resulting from amplified expression of phosphorylated PKC due to cholesterol depletion is conceivably the driving force for increase in cell stiffness.

The differences in phosphorylated PKC and the ensuing changes in actin polymerization, led us to further investigate the changes in cell spreading in greater detail. The cells were allowed to spread on collagen coated glass slides for 3 hours. After 3 hours, cholesterol depleted cells demonstrated ~26% increase in

spread area and ~33% increase in the aspect ratio as compared to untreated cells, implying that the cells exhibit enhanced spreading and are more elongated (Fig. 4A). Cholesterol enriched cells were more rounded, with a modest decrease in spread area (~5%) and aspect ratio (~17%) in comparison to untreated control (Fig. 4A). We can attribute the differences in spreading behavior in cholesterol depleted cells, to the enhanced levels of phosphorylated PKC due to treatment with MβCD. Higher degree of actin polymerization plausibly enables the cholesterol depleted cells to demonstrate increased spreading. On the other hand, lower expression of phosphorylated PKC in enriched cells conceivably translates to diminished polymerization of actin.

PKC activation is amplified in the presence of chemokines (Konishi et al., 1997). We assessed the changes in response to the chemokine MCP-1 which is a physiologically important chemoattractant for monocytes (Deshmane, Kremlev, Amini, & Sawaya, 2009). Upon stimulation with MCP-1, the overall levels of phosphorylated PKC were elevated for all the conditions. Cholesterol depleted cells exhibited ~136% higher expression of phosphorylated PKC, whereas cholesterol enrichment resulted in a decrease of ~91%, as compared to untreated THP-1 cells (Fig. 3). Using confocal microscopy, we visualized the morphological changes in THP-1 cells while undergoing chemotaxis in response to MCP-1. Cholesterol depleted cells exhibited an elongated cell shape as compared to untreated THP-1 cells (Fig. 4B), and the elongation is due to cytoskeletal rearrangement in these cells resulting from enhanced expression of phosphorylated PKC. Cholesterol enriched cells on the other hand, expectedly, had a significantly reduced expression of F-actin (green; Fig. 4B), possibly resulting from reduced expression of phosphorylated PKC (Fig. 3), which is also reflected in its spreading behavior (Fig. 4A). The decreased actin polymerization plausibly causes the cholesterol enriched cells to be more deformable.

In summary, we have demonstrated the bearing of cellular cholesterol content on the biomechanical response of human monocytic cell line THP-1 cells. Our data show that the cellular cholesterol content governs cellular deformability as a consequence of PKC phosphorylation, which directly orchestrates

several important downstream signaling pathways. The changes in cellular deformability can have significant implications in monocyte immune response including interaction with the vascular endothelium, transmigration into tissues, and phagocytosis [Chen et al., 2016; Fu, He, Li, Shyy, & Zhu, 2010; Najafinobar et al., 2016]. Monocytes are vital components of the immune system and assessment of biomechanical response at the cellular level can help better understand the mechanistic aspects of infection and inflammation.

Acknowledgment

The authors would like to thank Dr. Anand Srinivasan and Dr. Shankar J. Evani for technical assistance. The authors would like to acknowledge the assistance of the Kleberg Advanced Microscopy Center facility and the RCMI Biophotonics Core Facility at The University of Texas at San Antonio, supported by the National Institute on Minority Health and Health Disparities of the National Institutes of Health under Award Number G12MD007591.

Conflict of interest statement

The authors declare no conflict of interest.

Funding

This work was supported by a grant from the NIH (HL112629).

References

Barman, S., & Nayak, D. P. (2007). Lipid raft disruption by cholesterol depletion enhances influenza a virus budding from MDCK cells. *Journal of Virology, 81*(22), 12169-12178. doi: 10.1128/Jvi.00835-07

Bunnell, S. C., Kapoor, V., Trible, R. P., Zhang, W. G., & Samelson, L. E. (2001). Dynamic actin polymerization drives T cell receptor-induced spreading: A role for the signal transduction adaptor LAT. *Immunity, 14*(3), 315-329. doi: Doi 10.1016/S1074-7613(01)00112-1

Byfield, F. J., Aranda-Espinoza, H., Romanenko, V., Rothblat, G., Hammer, D. A., & Levitan, I. (2004). Cholesterol depletion results in stiffening of aortic endothelial cells as determined by micropipette aspiration analysis and traction force microscopy. *Journal of General Physiology, 124*(1), 15a-16a.

Cabrera-Poch, N., Sanchez-Ruiloba, L., Rodriguez-Martinez, M., & Iglesias, T. (2004). Lipid raft disruption triggers protein kinase C and Src-dependent protein kinase D activation and Kidins220 phosphorylation in neuronal cells. *Journal of Biological Chemistry, 279*(27), 28592-28602. doi: 10.1074/jbc.M312242200

Chen, J., Zhou, W., Jia, Q., Zhang, S., Yao, W., Wei, F., . . . Wang, N. (2016). Efficient extravasation of tumor-repopulating cells depends on cell deformability. [Research Support, N.I.H., Extramural

Research Support, Non-U.S. Gov't]. *Sci Rep, 6*, 19304. doi: 10.1038/srep19304

Deshmane, S. L., Kremlev, S., Amini, S., & Sawaya, B. E. (2009). Monocyte Chemoattractant Protein-1 (MCP-1): An Overview. *Journal of Interferon and Cytokine Research, 29*(6), 313-326. doi: 10.1089/jir.2008.0027

Dy, M. C., Kanaya, S., & Sugiura, T. (2013). Localized cell stiffness measurement using axial movement of an optically trapped microparticle. *J Biomed Opt, 18*(11), 111411. doi: 10.1117/1.JBO.18.11.111411

Etienne, J., & Duperray, A. (2011). Initial Dynamics of Cell Spreading Are Governed by Dissipation in the Actin Cortex. *Biophys J, 101*(3), 611-621. doi: 10.1016/j.bpj.2011.06.030

Foster, G. A., Gower, R. M., Stanhope, K. L., Havel, P. J., Simon, S. I., & Armstrong, E. J. (2013). On-chip phenotypic analysis of inflammatory monocytes in atherogenesis and myocardial infarction. [Research Support, N.I.H., Extramural]. *Proc Natl Acad Sci U S A, 110*(34), 13944-13949. doi: 10.1073/pnas.1300651110

Fu, C., He, J., Li, C., Shyy, J. Y., & Zhu, Y. (2010). Cholesterol increases adhesion of monocytes to endothelium by moving adhesion molecules out of caveolae. [Research Support, Non-U.S. Gov't]. *Biochim Biophys Acta, 1801*(7), 702-710. doi: 10.1016/j.bbalip.2010.04.001

Hayashi, K., & Higaki, M. (2016). Stiffness of Intact Endothelial Cells from Fresh Aortic Bifurcations of Atherosclerotic Rabbits - Atomic Force Microscopic Study. *Journal of Cellular Physiology*. doi: 10.1002/jcp.25379

Helmreich, E. J. (2003). Environmental influences on signal transduction through membranes: a retrospective mini-review. [Review]. *Biophys Chem, 100*(1-3), 519-534.

Kabouridis, P. S., Janzen, J., Magee, A. L., & Ley, S. C. (2000). Cholesterol depletion disrupts lipid rafts and modulates the activity of multiple signaling pathways in T lymphocytes. *European Journal of Immunology, 30*(3), 954-963. doi: Doi 10.1002/1521-4141(200003)30:3<954::Aid-Immu954>3.3.Co;2-P

Konishi, H., Tanaka, M., Takemura, Y., Matsuzaki, H., Ono, Y., Kikkawa, U., & Nishizuka, Y. (1997). Activation of protein kinase C by tyrosine phosphorylation in response to H2O2. [Research Support, Non-U.S. Gov't]. *Proc Natl Acad Sci U S A, 94*(21), 11233-11237.

Kwik, J., Boyle, S., Fooksman, D., Margolis, L., Sheetz, M. P., & Edidin, M. (2003). Membrane cholesterol, lateral mobility, and the phosphatidylinositol 4,5-bisphosphate-dependent organization of cell actin. *Proc Natl Acad Sci U S A, 100*(24), 13964-13969. doi: DOI 10.1073/pnas.2336102100

Liu, M. L., Reilly, M. P., Casasanto, P., McKenzie, S. E., & Williams, K. J. (2007). Cholesterol enrichment of human monocyte/macrophages induces surface exposure of phosphatidylserine and the release of biologically-active tissue factor-positive microvesicles. [Research Support, N.I.H., Extramural]. *Arterioscler Thromb Vasc Biol, 27*(2), 430-435. doi: 10.1161/01.ATV.0000254674.47693.e8

Lundbaek, J. A., Andersen, O. S., Werge, T., & Nielsen, C. (2003). Cholesterol-induced protein sorting: an analysis of energetic feasibility. [Evaluation Studies

Research Support, Non-U.S. Gov't

Research Support, U.S. Gov't, P.H.S.]. *Biophys J, 84*(3), 2080-2089. doi: 10.1016/S0006-3495(03)75015-2

Mason, R. P., Herbette, L. G., & Tulenko, T. N. (1993). Cholesterol Enrichment during Dietary Atherosclerosis Alters Smooth-Muscle Plasma-Membrane Width and Structure - Evidence for Reversal by the 1,4-Dihydropyridine Amlodipine. *Calcium Antagonists : Pharmacology and Clinical Research, 3*, 149-155.

Mellado, M., Rodriguez-Frade, J. M., Aragay, A., del Real, G., Martin, A. M., Vila-Coro, A. J., . . . Martinez-A, C. (1998). The chemokine monocyte chemotactic protein 1 triggers Janus kinase 2 activation and tyrosine phosphorylation of the CCR2B receptor. *Journal of Immunology, 161*(2), 805-813.

Najafinobar, N., Mellander, L. J., Kurczy, M. E., Dunevall, J., Angerer, T. B., Fletcher, J. S., & Cans, A. S. (2016). Cholesterol Alters the Dynamics of Release in Protein Independent Cell Models for Exocytosis. *Sci Rep, 6*, 33702. doi: 10.1038/srep33702

Oh, H., Mohler, E. R., 3rd, Tian, A., Baumgart, T., & Diamond, S. L. (2009). Membrane cholesterol is a biomechanical regulator of neutrophil adhesion. [Research Support, N.I.H., Extramural]. *Arterioscler Thromb Vasc Biol, 29*(9), 1290-1297. doi: 10.1161/ATVBAHA.109.189571

Oh, K. W., Lee, K., Ahn, B., & Furlani, E. P. (2012). Design of pressure-driven microfluidic networks using electric circuit analogy. *Lab on a Chip, 12*(3), 515-545. doi: 10.1039/c2lc20799k

Pande, G. (2000). The role of membrane lipids in regulation of integrin functions. *Current Opinion in Cell Biology, 12*(5), 569-574. doi: Doi 10.1016/S0955-0674(00)00133-2

Rask-Madsen, C., & King, G. L. (2005). Proatherosclerotic mechanisms involving protein kinase C in diabetes and insulin resistance. [Research Support, N.I.H., Extramural

Research Support, Non-U.S. Gov't

Research Support, U.S. Gov't, P.H.S.

Review]. *Arterioscler Thromb Vasc Biol, 25*(3), 487-496. doi: 10.1161/01.ATV.0000155325.41507.e0

Roduit, C., van der Goot, F. G., De Los Rios, P., Yersin, A., Steiner, P., Dietler, G., . . . Kasas, S. (2008). Elastic membrane heterogeneity of living cells revealed by stiff nanoscale membrane domains. [Research Support, Non-U.S. Gov't]. *Biophys J, 94*(4), 1521-1532. doi: 10.1529/biophysj.107.112862

Salker, M. S., Schierbaum, N., Alowayed, N., Singh, Y., Mack, A. F., Stournaras, C., . . . Lang, F. (2016). LeftyA decreases Actin Polymerization and Stiffness in Human Endometrial Cancer Cells. *Sci Rep, 6*, 29370. doi: 10.1038/srep29370

Shelby, J. P., White, J., Ganesan, K., Rathod, P. K., & Chiu, D. T. (2003). A microfluidic model for single-cell capillary obstruction by Plasmodium falciparum-infected erythrocytes. [Research Support, Non-U.S. Gov't

Research Support, U.S. Gov't, P.H.S.]. *Proc Natl Acad Sci U S A, 100*(25), 14618-14622. doi: 10.1073/pnas.2433968100

Shima, T., Nada, S., & Okada, M. (2003a). Transmembrane phosphoprotein Cbp senses cell adhesion signaling mediated by Src family kinase in lipid rafts. [Research Support, Non-U.S. Gov't]. *Proc Natl Acad Sci U S A, 100*(25), 14897-14902. doi: 10.1073/pnas.2432139100

Shima, T., Nada, S., & Okada, M. (2003b). Transmembrane phosphoprotein Cbp senses cell adhesion signaling mediated by Src family kinase in lipid rafts. *Proceedings of the National Academy of Sciences of the United States of America, 100*(25), 14897-14902. doi: 10.1073/pnas.2432139100

Sun, M., Northup, N., Marga, F., Huber, T., Byfield, F. J., Levitan, I., & Forgacs, G. (2007). The effect of cellular cholesterol on membranecytoskeleton adhesion. *Journal of Cell Science, 120*(13), 2223-2231. doi: 10.1242/jcs.001370

Thomas, G., Burnham, N. A., Camesano, T. A., & Wen, Q. (2013). Measuring the mechanical properties of living cells using atomic force microscopy. [Video-Audio Media]. *J Vis Exp*(76). doi: 10.3791/50497

Xing, Y. H., Gu, Y., Xu, L. C., Siedlecki, C. A., Donahue, H. J., & You, J. (2011). Effects of Membrane Cholesterol Depletion and GPI-Anchored Protein Reduction on Osteoblastic Mechanotransduction. *Journal of Cellular Physiology, 226*(9), 2350-2359. doi: Doi 10.1002/Jcp.22579

Xu, W. W., Mezencev, R., Kim, B., Wang, L. J., McDonald, J., & Sulchek, T. (2012). Cell Stiffness Is a Biomarker of the Metastatic Potential of Ovarian Cancer Cells. *PLoS One, 7*(10). doi: ARTN e46609 DOI 10.1371/journal.pone.0046609.

Figure and Table Legends

Fig. 1. Membrane fluidity of THP-1 cells estimated using the fluorescent probe PDA. * represents statistically significant difference ($p < 0.05$, n = 3) in comparison to untreated cells.

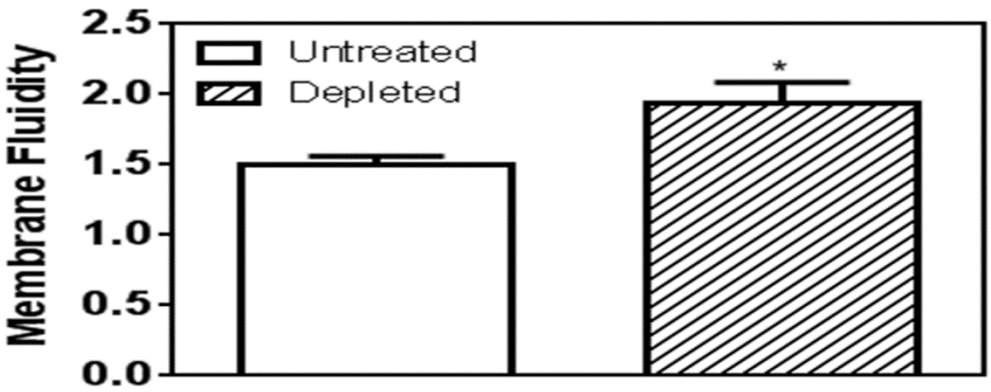

Fig. 2. Estimation of cellular deformability using custom microfluidic device. (A) Schematic of microfluidic channel design. (B) Estimation of deformability parameters of THP-1 cells. * represents statistically significant difference (p< 0.05, n = 3) in comparison to untreated cells.

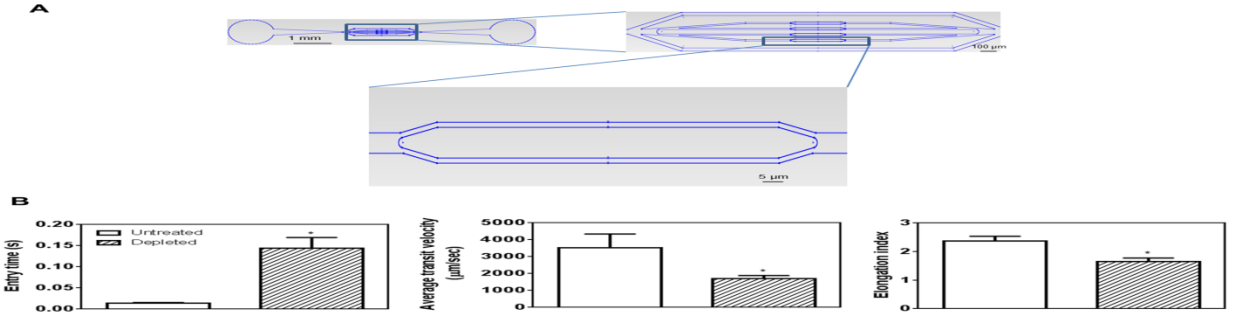

Fig. 3. Estimation of cytoskeletal reorganization in THP-1 cells. Phosphorylated PKC was measured with and without MCP-1 stimulus. Immunoblot analysis was carried out using antiphosphotyrosine antibody (PY20) and anti β actin. After densitometric analysis of the blots, data was expressed as fold phosphorylation over basal level. The result is representative of two independent experiments.

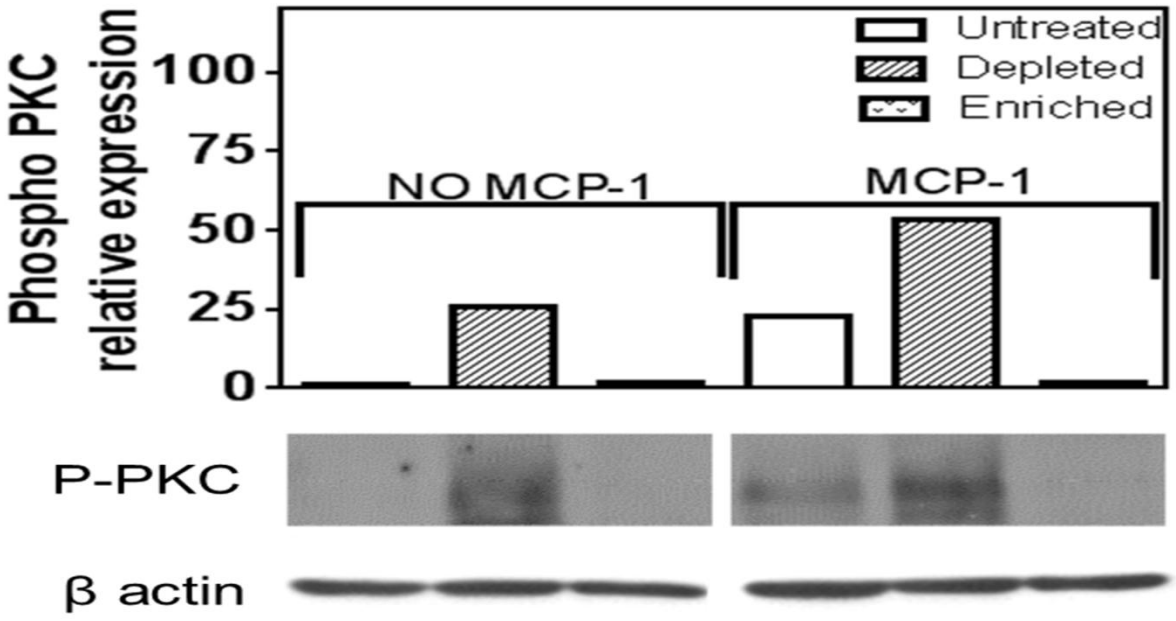

Fig. 4. Changes in THP-1 cell morphology due to cellular cholesterol content. (A) Scanning electron microscopy images of THP-1 cells spread on collagen coated glass slides after 3 hours. * & ϕ represent statistically significant difference ($p< 0.05$, n = 3) in comparison to untreated and depleted cells, respectively. (B) Changes in THP-1 cell shape while passing through transwell pores in response to MCP-1. Actin is shown in green and the nucleus is shown in blue.

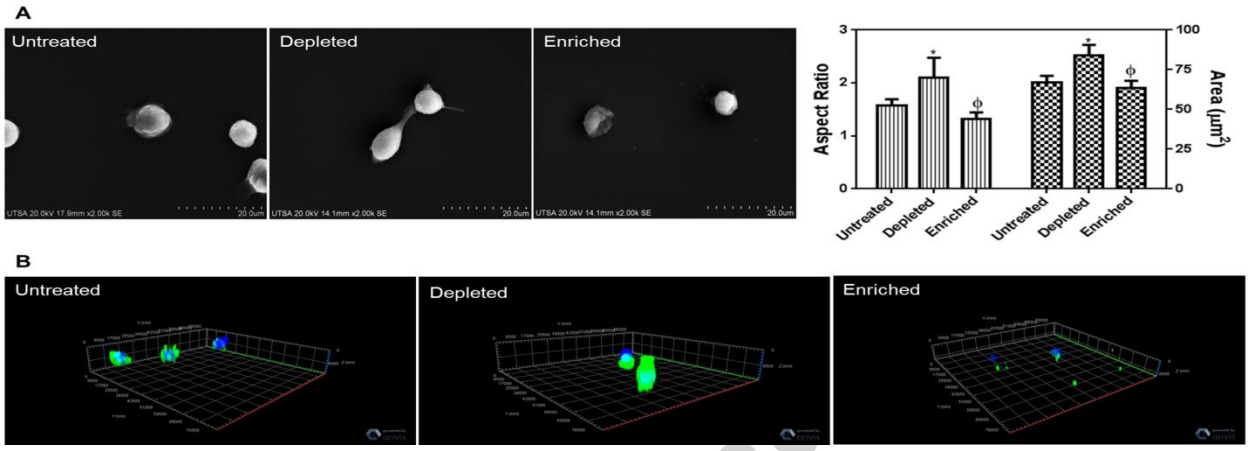

Table 1. Cholesterol content in THP-1 cells: whole cell and plasma membrane.

	Cholesterol content in whole cell (μg/ml)	Cholesterol content in plasma membrane (μg/ml)	% cellular cholesterol in plasma membrane
Untreated	1.257	1.091	86.794
Depleted (5 mM)	0.633	0.546	86.256

Depleted (10 mM)	0.413	0.345	83.535

Supplementary Section

Fig. S1. Perfusion of an untreated cell through the microfluidic device. Scale bar (red) is 5 μm.

Fig. S2. Estimation of THP-1 cellular deformability using atomic force microscopy (AFM). * & ϕ represent statistically significant difference ($p < 0.05$, n = 3) in comparison to depleted and untreated cells, respectively.